Inorg. Chem. **2003**, *42*, 5293–5303

Magnetic and Optical Studies on an $S = 6$ Ground-State Cluster $[Cr_{12}O_9(OH)_3(O_2CCMe_3)_{15}]$: Determination of, and the Relationship Between, Single-Ion and Cluster Spin Hamiltonian Parameters

David Collison,[†] Mark Murrie,[‡] Vasily S. Oganesyan,[§] Stergios Piligkos,[†] Nigel R. J. Poolton,[||] Gopalan Rajaraman,[†] Graham M. Smith,[||] Andrew J. Thomson,[§] Grigore A. Timko,[⊥] Wolfgang Wernsdorfer,[#] Richard E. P. Winpenny,[†] and Eric J. L. McInnes*,[†]

Department of Chemistry, The University of Manchester, Oxford Road, Manchester M13 9PL, U.K., Department für Chemie und Biochemie, Universität Berne, CH-3000 Bern 9, Switzerland, School of Chemical Sciences, University of East Anglia, Norwich NR4 7TJ, U.K., School of Physics and Astronomy, University of St. Andrews, St. Andrews, Fife KY16 9SS, U.K., Institute of Chemistry, Moldovan Academy of Sciences, Kishinev MD-2028, Moldova, and Laboratoire de Magnétisme Louis Néel, CNRS, BP 166, 38042 Grenoble Cedex 9, France

Received May 19, 2003

The dodecametallic Cr(III) cluster $[Cr_{12}O_9(OH)_3(O_2CCMe_3)_{15}]$ has a ground spin state of $S = 6$ characterized by the spin Hamiltonian parameters $g_{ZZ} = 1.965$, $g_{XX} = g_{YY} = 1.960$, $D_{S=6} = +0.088$ cm^{-1}, and $E_{S=6} = 0$ (where D and E are the axial and rhombic zero-field splitting parameters, respectively) as determined by multifrequency EPR spectroscopy and magnetization studies. Micro-SQUID magnetization studies reveal steps due to the fine structure of the ground state, with the spacing between the steps in excellent agreement with the $D_{S=6}$ value determined by EPR. Analysis of high-resolution optical data (MCD) allows us to determine the single-ion g values and D value ($= -1.035$ cm^{-1}) of the constituent Cr(III) ions directly. A vector coupling analysis demonstrates that the cluster ZFS is almost entirely due to the single-ion component. Thus, the relative orientations of the local and cluster magnetic axes can lead to a cluster ZFS of *opposite* sign to the single-ion value, even when this is the only significant contribution.

Introduction

There has been great interest in molecules with large ground-state spin (S) since the discovery that such molecules, when combined with a significant negative zero-field splitting (ZFS, D_S) within this ground state, can lead to the phenomenon of single-molecule magnetism (SMM).[1] In such molecules there is a barrier to relaxation (reorientation) of spin, the magnitude of which is given by $|D_S|S^2$. This leads to magnetic hysteresis of an entirely molecular origin at low temperatures and the possibility of storing information in single molecules.[2] Moreover, the observation of magnetization quantum tunneling effects[3] has led to the proposal that SMMs could be exploited as Qbits in quantum computing.[4] The original discovery was in a dodecametallic, mixed-valence manganese cluster $[Mn_{12}O_{12}(O_2CMe)_{16}(H_2O)_4]$, trivially known as "$Mn_{12}$", which has an $S = 10$ ground state with an axial ZFS of -0.42 K.[1] Because the temperature below which SMMs operate is controlled in large part by the product $|D_S|S^2$, where D_S is *negative* in sign, a primary goal in this field is to maximize S and $|D_S|$. This requires a detailed understanding of the factors that control these parameters. Large S can arise from ferri- or ferromagnetic exchange in polymetallic complexes of paramagnetic transi-

* Corresponding author. E-mail: eric.mcinnes@man.ac.uk. Fax: +44-161-275-4598.
[†] The University of Manchester.
[‡] Universität Berne.
[§] University of East Anglia.
[||] University of St. Andrews.
[⊥] Moldovan Academy of Sciences.
[#] Laboratoire de Magnétisme Louis Néel, CNRS.

(1) (a) Sessoli, R.; Tsai, H.-L.; Shake, A. R.; Wang, S.; Vincent, J. B.; Folting, K.; Gatteschi, D.; Christou, G.; Hendrickson, D. N. *J. Am. Chem. Soc.* **1993**, *115*, 1804. (b) Sessoli, R.; Gatteschi, D.; Caneschi, A.; Novak, M. A. *Nature* **1993**, *365*, 141.
(2) Christou, G.; Gatteschi, D.; Hendrickson, D. N.; Sessoli, R. *MRS Bull.* **2000**, *25*, 66 and references therein.
(3) (a) Thomas, L.; Lionti, F.; Ballou, R.; Gatteschi, D.; Sessoli, R.; Barbara, B. *Nature* **1996**, *383*, 145. (b) Wernsdorfer, W.; Aliaga-Alcade, N.; Hendrickson, D. N.; Christou, G. *Nature* **2002**, *416*, 406.
(4) Leuenberger, M. N.; Loss, D. *Nature* **2001**, *410*, 789.

10.1021/ic034541b CCC: $25.00
Published on Web 07/26/2003

tion metal ions, and molecules with ground state S up to $^{33}/_2$, $^{39}/_2$, or $^{51}/_2$ have been reported.[5] Cluster ZFSs are less predictable as there are many competing factors: the single-ion ZFS, anisotropic and dipolar exchange, and relative orientations of the single ions and the cluster magnetic axes. To control D_S it is first necessary to quantify the importance of these factors.

The ideal way to quantify the single-ion ZFS (D) is to dope the appropriate paramagnetic ion into an isostructural and diamagnetic analogue of the cluster. D can then be determined directly by electron paramagnetic resonance (EPR) spectroscopy. A simple, but very elegant, example of this approach is the work of Kremer on the antiferromagnetically coupled Cr(III) dimers $[LCr(OH)_3CrL]^{3+}$ (L = tridentate ligand), where the ZFSs of the $S = 1, 2, 3$ excited states were all observable by EPR.[6] The analogous {CoCo} dimer could also be made, and doping Cr(III) into this allowed direct measurement of the single-ion ZFS for the system. Abbati et al.[7] demonstrated the utility of this approach to larger clusters in the cyclic hexametallic Fe(III) complex $[Fe_6(OCH_3)_{12}(pmdpm)_6]$ (Hpmdpm = 1,3-bis(4-methoxyphenyl)-1,3-propanedione) by doping Fe(III) into the diamagnetic $\{Ga_6\}$ analogue. Unfortunately, for more complicated clusters, this direct approach often becomes impossible because the appropriate diamagnetic analogue cannot be made. Some workers have made the approximation that the single-ion parameters can be estimated from simple monomeric complexes where the metal ion has a similar coordination sphere. The single-ion ZFS can then be projected on to the cluster ground-state ZFS using the vector coupling techniques detailed by Bencini and Gatteschi.[8] For example, Barra et al.[9] used this methodology to conclude that the ground state $D_{S=10}$ in Mn_{12} itself is largely due to the single-ion anisotropy of the Mn(III) ions, which they assumed to be similar to that observed in $[Mn(dbm)_3]$ (Hdbm = 1,3-diphenyl-1,3-propanedione).[10] The same group have used empirical angular overlap model calculations to estimate the single-ion D in Fe(III) clusters.[11] It would be far preferable to have a more direct measurement of the single-ion ZFS.

Several authors have attempted to interpret ZFS in *monomeric* species within a ligand field theory framework and hence in terms of optical data. For the specific example of the Cr(III) ion, closed-form analytical expressions have been developed for the ZFS of the $^4A_2$ ground state in terms of the optical excited states that can be mixed in via spin−orbit coupling.[12−17] The most successful model is that described by Macfarlane that considers all possible excited states of the d^3 configuration that make a contribution to D in a third-order perturbation treatment, including both the spin quartet and doublet states.[18] To exploit these formulas, it is necessary to have good-quality (high-resolution) optical data. Fortunately, spin-forbidden (and therefore weak) optical transitions to the spin doublet states can often be enhanced relative to the spin-allowed transitions in magnetic circular dichroism (MCD) spectra.[19] Enhancement of these transitions via magnetic exchange interactions has also been observed in absorption spectra of Cr(III) dimers[20] and trimers.[21]

In this work, we report the magnetic characterization of the dodecametallic Cr(III) cluster $[Cr_{12}O_9(OH)_3(O_2CCMe_3)_{15}]$ (**1**) (Figure 1) by multifrequency (9−180 GHz) EPR spectroscopy and micro-SQUID magnetometry, and demonstrate that **1** has an $S = 6$ ground state. The micro-SQUID magnetization studies reveal a stepped structure due to the fine structure of the ground state, the first time this effect has been observed. We then demonstrate that optical (UV/visible absorption and MCD) studies of large clusters can be used to determine the *single-ion* ZFSs directly by treating the system as a pseudomonomeric Cr(III) ion and applying Macfarlane's model to the experimentally determined excited-state energies. Using this method, and by application of the vector coupling approach, we find that the ground-state ZFS of **1**, as determined by multifrequency EPR, is almost exclusively due to the single-ion Cr(III) contributions. Furthermore, we demonstrate that the relative orientations of the local and cluster magnetic axes are *as important* as the single-ion ZFSs in determining the sign of the cluster ZFS. Some of these results have appeared in a preliminary communication.[22]

Experimental Section

1 was made as reported previously.[22,23]

EPR spectra were measured on powders and frozen solutions (CH_2Cl_2/toluene, 10:1 v/v) of **1** at about 9 (X-), 24 (K-), and 34 GHz (Q-band) on a Bruker ESP 300E spectrometer. The 90 and

(5) (a) Goodwin, J. C.; Sessoli, R.; Gatteschi, D.; Wernsdorfer, W.; Powell, A. K.; Heath, S. L. *J. Chem. Soc., Dalton Trans.* **2000**, 1835. (b) Zhong, Z. J.; Seino, H.; Mizobe, Y.; Hidai, M.; Fujishima, A.; Ohkoshi, S.; Hashimoto, K. *J. Am. Chem. Soc.* **2000**, *122*, 2952. (c) Larianova, J.; Gross, M.; Pilkington, M.; Andres, H.; Stoekli-Evans, H.; Güdel, H. U.; Decurtins, S. *Angew. Chem., Int. Ed.* **2000**, *39*, 1605.

(6) (a) Kremer, S. *Inorg. Chem.* **1985**, *24*, 887. (b) Glerup, J.; Larsen, S.; Weihe, H. *Acta Chim. Scand.* **1993**, *47*, 1154.

(7) Abbati, G. L.; Brunel, L.-C.; Casalta, H.; Cornia, A.; Fabretti, A. C.; Gatteschi, D.; Hassan, A. K.; Jansen, A. G. M.; Maniero, A. L.; Pardi, L.; Paulsen, C.; Segre, U. *Chem. Eur. J.* **2001**, *7*, 1796.

(8) Bencini, A.; Gatteschi, D. *EPR of Exchange Coupled Systems*; Springer-Verlag: Berlin, 1989.

(9) Barra, A.-L.; Gatteschi, D.; Sessoli, R. *Phys. Rev. B* **1997**, *56*, 8192.

(10) Barra, A.-L.; Gatteschi, D.; Sessoli, R.; Abbati, G. L.; Cornia, A.; Fabretti, A. C.; Uytterhoeven, M. G. *Angew. Chem., Int. Ed. Engl.* **1997**, *36*, 2329.

(11) Barra, A.-L.; Caneschi, A.; Cornia, A.; de Biani, F. F.; Gatteschi, D.; Sangregorio, C.; Sessoli, R.; Sorace, L. *J. Am. Chem. Soc.* **1999**, *121*, 5302.

(12) Sugano, S.; Peter, M. *Phys. Rev.* **1961**, *122*, 381.

(13) McGarvey, B. R. *J. Chem. Phys.* **1964**, *41*, 3743.

(14) Garrett, H. B.; DeArmond, K.; Gutowsky, H. S. *J. Chem. Phys.* **1966**, *44*, 3393.

(15) Abragam, A.; Bleaney, B. *Electron Paramagnetic Resonance of Transition Ions*; Clarendon Press: Oxford, 1970; p 430.

(16) Mohrmann, L. E., Jr; Garrett, B. B. *Inorg. Chem.* **1974**, *13*, 357.

(17) Pedersen, E.; Toftlund, H. *Inorg. Chem.* **1974**, *13*, 1603.

(18) Macfarlane, R. M. *J. Chem. Phys.* **1967**, *47*, 2066.

(19) (a) McCaffery, A. J.; Stephens, P. J.; Schatz, P. N. *Inorg. Chem.* **1967**, *6*, 1614. (b) Harding, M. J.; Briat, B. *Mol. Phys.* **1974**, *27*, 1153.

(20) Reber, C.; Güdel, H. U.; Spiccia, L.; Marty, W. *Inorg. Chem.* **1987**, *26*, 3186.

(21) Dubicki, L.; Day, P. *Inorg. Chem.* **1972**, *11*, 1868.

(22) (a) Mabbs, F. E.; McInnes, E. J. L.; Murrie, M.; Parsons, S.; Smith, G. M.; Wilson, C. C.; Winpenny, R. E. P. *Chem. Commun.* **1999**, 643. (b) Collison, D.; Oganesyan, V. S.; Piligkos, S.; Thomson, A. J.; Winpenny, R. E. P.; McInnes, E. J. L. *J. Am. Chem. Soc.* **2003**, *125*, 1168.

(23) Batsanov, A. S.; Timko, G. A.; Struchkov, N. V.; Gérbéléu, N. V.; Indrichan, K. M. *Koord. Khim.* **1991**, *17*, 662.

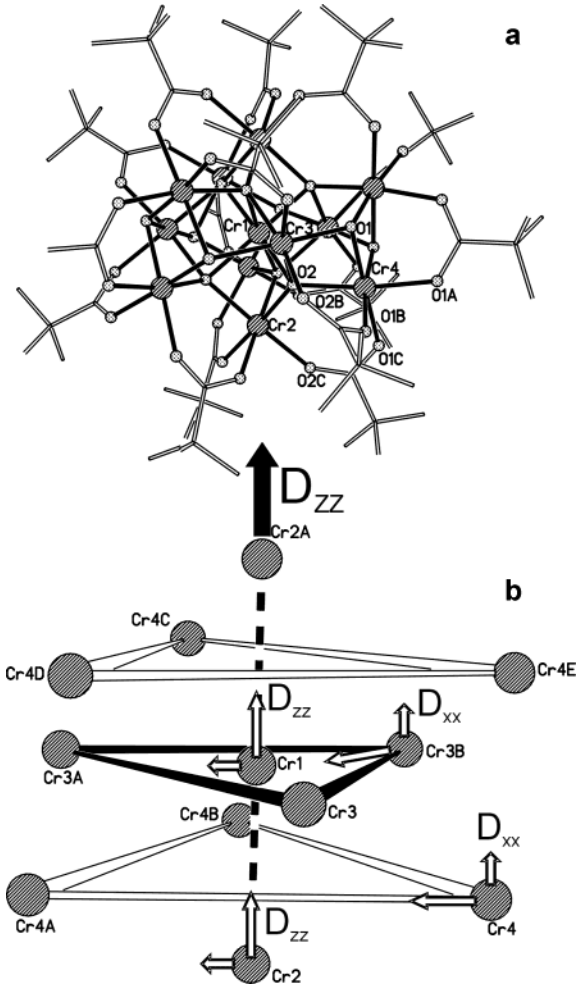

Figure 1. (a) Crystal structure of **1** and (b) view of the Cr_{12} skeleton emphasizing the penta-capped, trigonal prismatic core, the numbering scheme for the four crystallographically independent Cr(III) sites, and the relative orientations of the single-ion and cluster ZFS axes.

180 GHz EPR spectra were measured on a home-built instrument.[24] EPR simulations were performed using in-house software.[25] UV/visible and MCD spectra were recorded on solutions of **1** in $CHCl_3$/toluene (1:1 v/v) using methods reported elsewhere.[26] Simulations of MCD magnetization curves used in-house software described elsewhere.[27]

Magnetic measurements were performed on a powder of **1**, sealed in a gelatin capsule, using a Quantum Design SQUID magnetometer. Magnetic susceptibilities were measured between 1.8 and 325 K in an external magnetic field of 0.1 T and corrected for diamagnetism. Magnetization data were measured at 1.8 K in magnetic fields up to 5 T. Low-temperature (0.04−7 K) single-crystal magnetization data were measured using an array of micro-SQUIDs developed at the LLN−CNRS in Grenoble using procedures detailed elsewhere.[28]

Results and Discussion

1 crystallizes in the *R*32 space group, and the molecule lies on a 32 site. This results in only one magnetically distinct molecule at any orientation of the crystal with respect to the applied magnetic field in single-crystal EPR and magnetization experiments (see later). The molecular structure of **1** is based on a centered, pentacapped trigonal prism of Cr(III) ions (Figure 1b), and the cluster has crystallographic D_3 symmetry. The two triangular face capping Cr(III) ions [Cr(2) and Cr(2A)] and the central Cr(III) ion [Cr(1)] are on the C_3 axis. The vectors between each of the rectangular face-capping Cr(III) ions [Cr(3) and symmetry equivalents] and the central ion define the three C_2 axes. Only the vertexes of the trigonal prism are in a general position [Cr(4) and symmetry equivalents]. Therefore, there are only four independent Cr(III) sites in the structure of **1**. The structure is held together by 9 oxides and 3 hydroxides, as determined by neutron diffraction,[22] and capped by 15 pivalate anions.

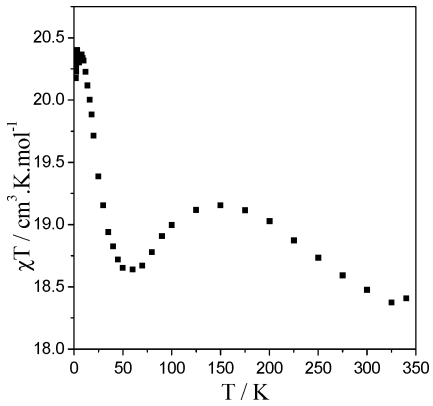

Figure 2. χT vs T for a powder sample of **1** measured in a 0.1 T magnetic field.

Susceptibility and Magnetization Studies. Magnetic susceptibility studies on a powder sample of **1** show two maximums in χT versus T (where χ is the molar magnetic susceptibility), at ∼10 and ∼150 K (Figure 2). At room temperature, $\chi T = 19.6$ cm^3 K mol^{-1}, lower than that expected for 12 noninteracting $S = {}^3/_2$ ions (21.6 cm^3 K mol^{-1} based on $g = 1.96$; see later). The lower temperature maximum is at a value of $\chi T = 21.6$ cm^3 K mol^{-1}. Although this value is that expected for 12 noninteracting Cr(III) ions, this is entirely coincidental as demonstrated by the nontrivial (non-Curie law) χT versus T curve. The value of χT can be explained by a large ground state S; $S = 6$ would give $\chi T = 20.2$ cm^3 K mol^{-1}. The complexity of the structure of **1** makes exact modeling of these data in terms of the possible exchange pathways impossible at present, and we restrict ourselves to the characterization of the ground spin state. Magnetization measurements performed on a powder sample of **1** at 1.8 K do not quite reach saturation at the maximum magnetic field strength employed of 5 T (Figure 3). However, it is clear that the plot is tending toward a saturation magnetization of $M_{sat} = 11.8\ \mu_B$, which is consistent with a ground-state spin of $S = 6$ with $g = 1.96$ (see below).

Magnetization measurements on a single crystal of **1** at temperatures below 0.5 K, and at magnetic field sweep rates above 0.07 T s^{-1}, reveal a narrow hysteresis. As EPR measurements demonstrate that the axial ZFS parameter of

(24) Smith, G. M.; Lesurf, J. C. G.; Mitchell, R. H.; Riedi, P. C. *Rev. Sci. Instrum.* **1998**, *69*, 3924.
(25) Mabbs, F. E.; Collison, D. *Mol. Phys. Rep.* **1999**, *26*, 39.
(26) Thomson, A. J.; Cheeseman, M. R.; George, S. J. *Methods Enzymol.* **1993**, *226*, 199.
(27) McInnes, E. J. L.; Pidcock, E.; Oganesyan, V. S.; Cheeseman, M. R.; Powell, A. K.; Thomson, A. J. *J. Am. Chem. Soc.* **2002**, *124*, 9219.
(28) Wernsdorfer, W. *Adv. Chem. Phys.* **2001**, *118*, 99.

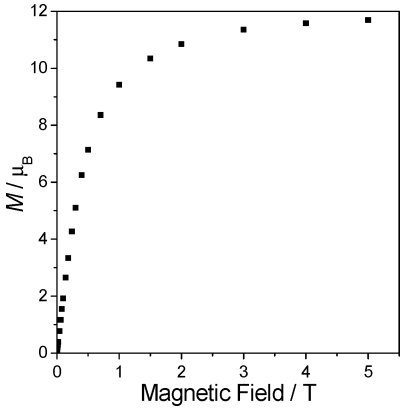

Figure 3. Magnetization vs magnetic field for a powder sample of **1**, measured at 1.8 K.

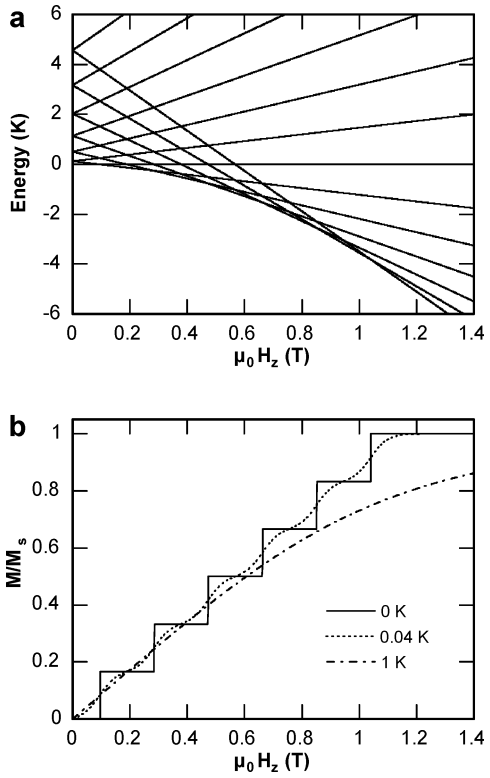

Figure 4. (a) Energy level diagram for the $S = 6$ ground state of **1** on application of a magnetic field parallel to the molecular Z (C_3) axis. (b) Calculated plot of magnetization vs magnetic field at 0, 0.04, and 1 K.

the ground state, $D_{S=6}$, is positive (see below), this hysteresis cannot be due to SMM behavior. In fact, it is due to a "phonon bottleneck"; i.e., the spin system cannot thermally equilibrate at the sweep rates used. Such behavior has been observed previously for a $\{V_{15}\}$ cage with an $S = {}^1/_2$ ground state,[29] where this effect has been used to estimate the effective tunnel splitting. Here, we use the phonon bottleneck effect to measure the magnetic field separation between M_S level crossings.

An energy level diagram for an $S = 6$ ground state with a positive, axial ZFS (see later) with the external magnetic field parallel to the molecular Z axis (the principal axis of the ZFS tensor or the "hard axis" of magnetization) is given

(29) Chiorescu, I.; Wernsdorfer, W.; Müller, A.; Bogge, H.; Barbara, B. *J. Magn. Magn. Mater.* **2000**, *221*, 103.

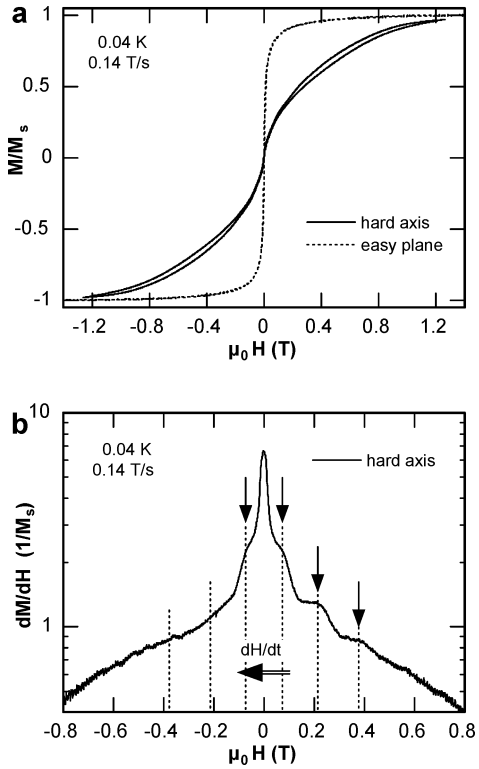

Figure 5. (a) Magnetization vs magnetic field for **1** measured on a micro-SQUID with the magnetic field applied parallel (hard axis) and perpendicular (easy plane) to the molecular Z (C_3) axis at 0.04 K and magnetic field sweep rate of 0.14 T s^{-1}. (b) Derivative of a part of the curve in (a) corresponding to the hard axis for the field sweep from 1.4 to −1.4 T.

in Figure 4. In principle, steps should be seen in a magnetization versus external magnetic field sweep when the M_S levels cross, i.e., when the ground state M_S changes from 0, 1, 2...6. Figure 4b shows calculated magnetization curves supposing a Boltzmann distribution among the M_S states. At very low temperatures, the six steps are seen clearly. However, at temperatures higher than 0.1 K, the steps are smeared out. If this step function could be observed experimentally, it would give a direct measure of $D_{S=6}$. For **1**, the Z axis is defined by symmetry to be the C_3 axis of the cluster and corresponds to the body diagonal of the diamond-shaped crystals. The experimental magnetization curve measured at 0.04 K using a micro-SQUID is shown in Figure 5, and a derivative of this curve reveals the presence of the steps (Figure 5b). The steps are only observed for the lower values of $|M_S|$ and are easier to observe as the field is swept toward zero. This behavior is due to a phonon bottleneck effect: the spin temperature decreases below the bath temperature (temperature of the cryostat) when the field is swept down to zero (adiabatic cooling) whereas it increases above the bath temperature when the field is swept up to high values. At much lower field sweep rates, the steps are not well resolved because in this case the spin temperature is always in equilibrium with the bath temperature. The separations between the steps in dM/dH versus H are ∼0.16 T. With the magnetic field parallel to the molecular Z axis, we would expect the steps to be separated by $2D_{S=6}$, which gives us $D_{S=6} \approx +0.08$ cm^{-1}. This value is in excellent agreement with that measured by EPR (see below).

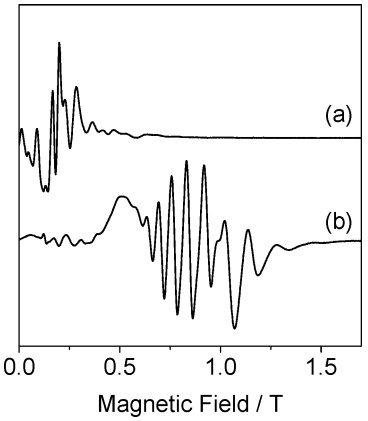

Figure 6. (a) X-band and (b) K-band EPR spectra of powdered samples of **1** at 4 K.

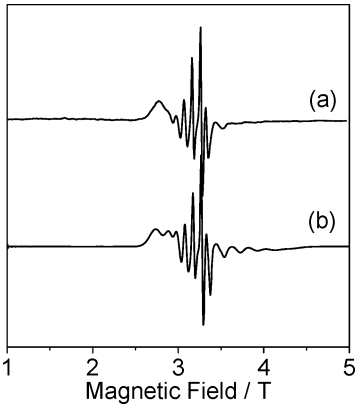

Figure 7. 90 GHz EPR spectra of a powdered sample of **1** at 4 K: (a) experimental and (b) simulation with the parameters in the text.

Stepped magnetization functions have been seen previously in antiferromagnetically coupled $\{Fe_{10}\}$ wheels,[30] but these are due to the ground S state changing as the magnetic field is increased ($S = 0$ in zero field and then $S = 1$, 2, etc., at specific values of applied field). We believe that the work here is the first example where steps between consecutive M_S levels within a given S state have been observed directly by magnetization measurements on a molecular system.

EPR Studies. The cluster ground-state spin Hamiltonian parameters S and D_S can be determined directly by EPR spectroscopy, where transitions are observed between the M_S substates of a given S manifold, as opposed to susceptibility techniques where a bulk response from a Boltzmann distribution over all spin states is measured. Where S, $|D_S|$, or both are large, it is often the case that the EPR spectrum spreads over several tesla in magnetic field and therefore high-frequency (90 GHz and above) EPR techniques, with their much larger possible magnetic field sweeps, are necessary.[31] Moreover, the large Zeeman splittings induced at large applied magnetic fields also allow determination of the sign of D_S by monitoring depopulation effects within a spin manifold.

At room temperature, powder samples of **1** give rise to a broad single line centered at $g = 1.96$. On cooling, this signal sharpens until at temperatures below ~40 K a highly structured multiplet is observed. At X-band, this spectrum is complicated (Figure 6a), but it simplifies considerably at K-band (Figure 6b), where a broad multiplet spreads from ~0.7 to over 1.8 T (the maximum field strength of the electromagnet), corresponding to formally allowed $\Delta M_S = \pm 1$ transitions within a large spin manifold, and there are weaker, spin-forbidden transitions that spread over the entire field range. A similar spectrum is observed at Q-band with slightly poorer resolution. The powder spectra are simplified further at 90 and 180 GHz (Figures 7a and 8a, respectively), with the formally forbidden transitions now at much lower magnetic fields and well separated from the formally allowed transitions. On cooling the sample from 40 to 2 K at 180 GHz, the transitions toward the high-field end of the multiplet decrease in intensity while those at the low-field end increase in intensity (Figure 8a). At 2 K and 180 GHz, only one transition is observed at ~6.2 T. These observations are all consistent with an isolated, large S ground state with $D_S < h\nu$ at all frequencies. Very similar spectra are observed from frozen CH_2Cl_2/toluene solutions of **1**—this demonstrates that the cluster remains intact in this solvent system.

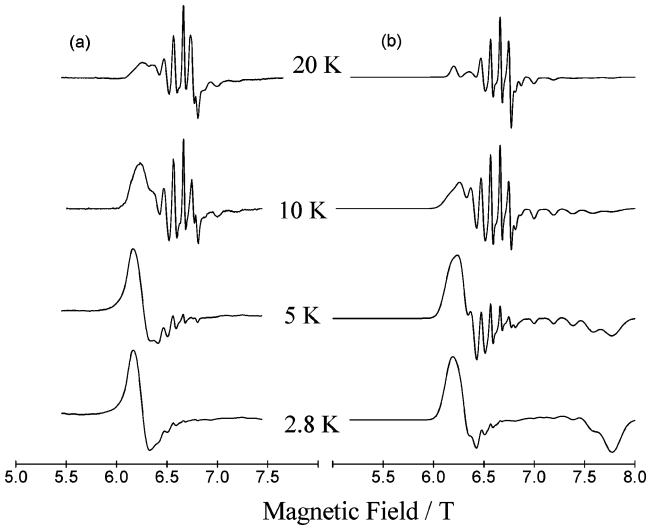

Figure 8. 180 GHz EPR spectra of a powdered sample of **1** between 20 and 1.8 K: (a) experimental and (b) simulated with the parameters in the text.

Simulation of the powder EPR spectra is necessary in order to determine S and also the g values and the magnitude and sign of the ZFS. The separations of the transitions in Figures 6−8 are ~0.09 T (~0.08 cm^{-1}), and we used this as an initial estimate of D_S. Good simulations of the powder spectra are possible with the spin Hamiltonian parameters $S = 6$, $g_{ZZ} = 1.965$, $g_{XX} = g_{YY} = 1.960$, $D_{S=6} = +0.088$ cm^{-1}, and $E_{S=6} = 0$ (where $D_{S=6}$ and $E_{S=6}$ are the axial and rhombic ZFS parameters, respectively and X, Y, Z refer to the *cluster* principal axes), and the 90 and 180 GHz simulations are shown in Figures 7b and 8b, respectively. Note that these axial parameters are consistent with the crystallographic D_3 symmetry of the cluster. The axial symmetry dictates that the most intense features in the experimental powder spectra (the multiplet centered at $g = 1.960$) are the "perpendicular"

(30) Taft, K. L.; Delfs, C. D.; Papaefthymiou, G. C.; Foner, S.; Gatteschi, D.; Lippard, S. J. *J. Am. Chem. Soc.* **1994**, *116*, 823.
(31) Barra, A. L.; Brunel, L. C.; Gatteschi, D.; Pardi, L.; Sessoli, R. *Acc. Chem. Res.* **1998**, *31*, 460.

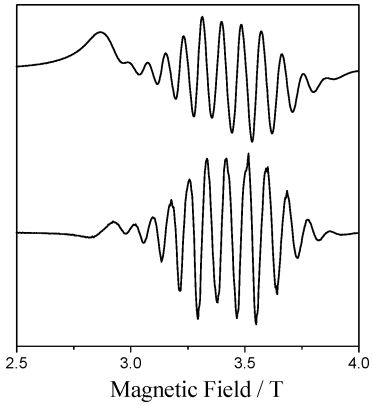

Figure 9. Single-orientation 90 GHz EPR spectrum of a single crystal of **1** at 10 K: first derivative (top) and second derivative (bottom).

transitions, i.e., arise from the subset of molecules with their unique axis (Z) perpendicular to the applied field. The "parallel" transitions are much weaker, broader, and poorly resolved in the powder spectra. However, despite the poor resolution of the parallel transitions, simulations with isotropic rather than axial g values give noticeably poorer fits to the experimental spectra. Simulations with other values of S between 4 and 8 also give much poorer fits. Final and conclusive evidence for the value of S comes from a single (arbitrary) orientation spectrum of a single crystal of **1** (Figure 9). The $\Delta M_S = \pm 1$ EPR selection rule predicts $2S$ allowed transitions at a given orientation. The 12 observed transitions in Figure 9 (number of maximums in second-derivative spectrum) define the ground state unambiguously as $S = 6$.

The sign of $D_{S=6}$ comes from modeling of depopulation effects within the $S = 6$ manifold at 180 GHz and between 20 and 2 K (Figure 8). Energy level diagrams calculated using the spin Hamiltonian parameters above and a positive $D_{S=6}$ value, for the applied magnetic field parallel to and perpendicular to the molecular Z axis (defined by symmetry to be the principal axis of the ZFS in the D_3 point group), are shown in Figure 10.

The 12 formally allowed EPR transitions at each orientation are shown for $\nu = 180$ GHz. On cooling the sample, the upper energy levels are depopulated in favor of the lower ones, resulting in skewing of the intensities of the EPR transitions within the $S = 6$ manifold. The most intense features of the powder spectra are the perpendicular transitions (see above). Within this perpendicular manifold, the transition arising from the ground M_S substate (which can be labeled $M_S = -6$ in the high-field limit) is the one at lowest field; hence, the intensity of this transition is enhanced on cooling the sample. Within the parallel manifold, the transition arising from the ground M_S state ($M_S = -6 \rightarrow -5$) is the one at highest field; hence, this transition is enhanced on cooling the sample. If the ZFS were negative, the highest and lowest field transitions in the perpendicular and parallel manifolds, respectively, would be enhanced on cooling. Variable-temperature simulations, which include the Boltzmann distribution of states, are in Figure 8b and confirm that $D_{S=6}$ is positive.

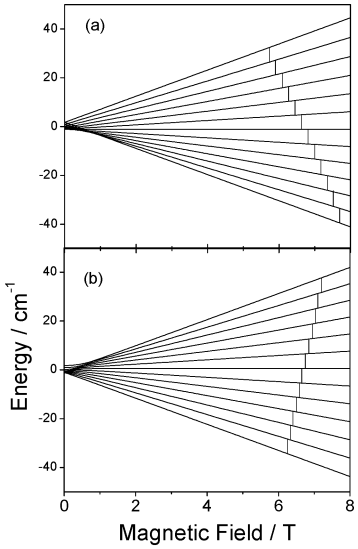

Figure 10. Energy level diagrams and allowed EPR transitions ($\nu = 180$ GHz) for the $S = 6$ ground state of **1** on application of an external magnetic field (a) parallel to and (b) perpendicular to the cluster C_3 axis.

Figures 6−8 illustrate how the spectral line widths are sharper at lower frequencies. It is also apparent that the line widths of the transitions within the $S = 6$ manifold are not constant at a given frequency: transitions are narrow in the center of the multiplet (~0.03 T at 180 GHz) and broaden severely in the wings (e.g., the solitary, remaining transition at 2 K and 180 GHz is ~0.2 T wide). This phenomenon has been observed previously for large S systems and has been ascribed to D strain;[32] i.e., there is a statistical distribution of D_S values rather than a single discrete value. Because the energy of each substate within the $S = 6$ manifold is given by $M_S^2 D_{S=6}$, there is a broader distribution of energies of the substate levels with higher $|M_S|$. Thus, there is a broader range of transition energies between high $|M_S|$ substates (i.e., transitions in the wings of the spectrum), and larger line widths are observed. Conversely, transitions between substates of small $|M_S|$ (in the middle of the spectrum) are much narrower. In the simulations in Figures 7 and 8, this has been modeled by calculating the line widths, $\Delta H = A + BM_S^2$. For example, at 180 GHz, the inherent line width is $A = 400$ G for Z (parallel) and 270 G for XY (perpendicular) transitions, with $B = 50$ G.

Optical Studies. The UV/visible spectrum of **1** in $CHCl_3$/toluene (1:1 v/v) at room temperature (Figure 11a) resembles that of monomeric Cr(III) with two d−d absorptions corresponding to the $^4A_2 \rightarrow {}^4T_2$ and a^4T_1 transitions (16 475 and 22 883 cm^{-1}, respectively). Note that we have labeled the optical transitions using terms appropriate for a single ion, and the appropriate energy level diagram[33] for a {Cr(III)-O_6} center is in Figure 12. The first of these transitions is expected to give Δ (or $10Dq$) directly for O_h symmetry ($\Delta = 16\,475$ cm^{-1}), and the Racah parameters B and C can be

(32) (a) Park, K.; Novotny, M. A.; Dalal, N. S.; Hill, S.; Rikvold, P. A. *Phys. Rev. B* **2001**, *65*, 014426. (b) Bouwen, A.; Caneschi, A.; Gatteschi, D.; Goovaerts, E.; Schoemaker, D.; Sorace, L.; Stefan, M. *J. Phys. Chem. B* **2001**, *105*, 2658.

(33) Macfarlane, R. M. *J. Chem. Phys.* **1963**, *39*, 3118.

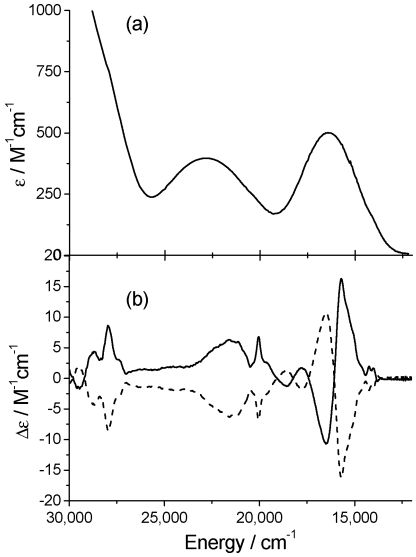

Figure 11. (a) UV/visible spectrum at 293 K; (b) MCD spectra at 1.8 K, and +5 (solid line) and −5 T (dashed line) magnetic fields, of **1** in $CHCl_3$/toluene (1:1 v/v) solution.

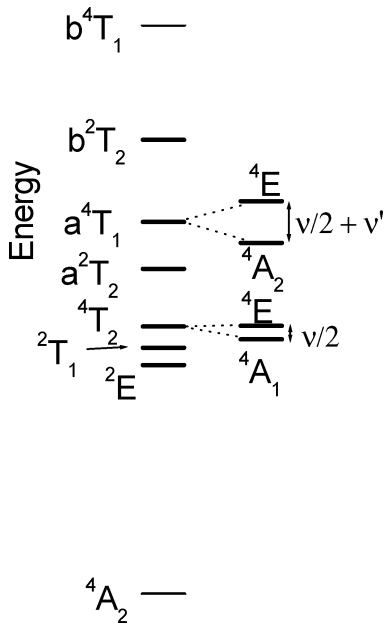

Figure 12. Optical ground and excited states for a monomeric {Cr(III)-O_6} center, after Macfarlane.[33]

calculated from this and the other transition energies (B = 534 cm^{-1}, $C \approx 3000$ cm^{-1}).[34]

The MCD spectrum at 1.8 K (Figure 11b) has much greater resolution than the room-temperature UV/visible spectrum (as has been observed previously for exchange coupled systems,[35] including large spin clusters[27]) and reveals that the $^4A_2 \rightarrow {}^4T_2$ band actually consists of two transitions at 16 502 and 15 673 cm^{-1}, assigned to $^4A_2 \rightarrow {}^4A_1$ and ^4E, respectively (see below), consistent with lowering from O_h to D_3 symmetry. Field-dependent MCD spectra of the transitions at 15 673 and 16 502 cm^{-1} were measured at 1.8 K (where only the $S = 6$ ground state is populated), and the resultant magnetization curves can be simulated to give the linear polarizations of the optical transitions. The transition at 15 673 cm^{-1} is found to be 91% *XY* polarized, consistent with assignment as $^4A_2 \rightarrow {}^4E$, while that at 16 502 cm^{-1} is 65% *XY* and 35% *XZ*(*YZ*) ($^4A_2 \rightarrow {}^4A_1$). These simulations assumed an $S = 6$ ground state and $D_{S=6} = +0.088$ cm^{-1} (as determined by EPR spectroscopy). Simulations based on $S = 5$ gave near identical curves, which suggests that MCD magnetization data are not sensitive enough to determine (or discriminate between different possible values of) large spin quantum numbers.

The $^4A_2 \rightarrow a^4T_1$ absorption at 22 880 cm^{-1} also consists of two transitions as witnessed by the unsymmetric UV/visible absorption profile and also by the significant shift compared to the MCD maximum in this region (21 598 cm^{-1}). The a^4T_1 state would be expected to be split in trigonal symmetry to $^4A_2$ and ^4E—we are only observing one of these transitions clearly in the MCD spectrum. A Gaussian fit to the absorption and the MCD spectrum is possible by assuming two components in this region at 21 598 and 24 154 cm^{-1}. The third spin-allowed transition $^4A_2 \rightarrow b^4T_1$ for Cr(III) would be expected at ~35 000 cm^{-1} (based on the calculated Racah parameters)—we do not observe this in the absorption or MCD spectra because it is presumably masked by charge-transfer transitions.

In addition to the formally spin-allowed transitions above, several sharper features are resolved in the MCD spectra that are not apparent in the UV/visible spectrum. These can be assigned to the spin-forbidden $^4A_2 \rightarrow {}^2E$ (14 085 cm^{-1}), $^4A_2 \rightarrow {}^2T_1$ (~15 150 cm^{-1}), $^4A_2 \rightarrow a^2T_2$ (20 000 cm^{-1}), and $^4A_2 \rightarrow b^2T_2$ (2 7933 cm^{-1}) transitions, where the assignment of the ordering of the states is based on that for other {Cr(III)-O_6} centers.[12,13,33] The transitions to b^2T_2 would be expected at ~30 000 cm^{-1} based on the calculated Racah parameters, and we assign the experimentally observed, sharp peak at 27 933 cm^{-1} accordingly. The enhancement of spin-forbidden quartet−doublet transitions in MCD has been observed previously for monomeric Cr(III) complexes.[19]

Relationship between Optical and EPR Data. (i) Zero-Field Splitting. Macfarlane[18] has given analytical expressions for the ground-state ZFS of trigonally distorted Cr(III) ions in terms of the energy gaps to the excited spin quartet and spin doublet states arising from the d^3 configuration (eq 1),

$$2D = \frac{4}{9}\left(\frac{1}{{\delta_3}^2} - \frac{1}{{\delta_1}^2}\right)\nu\zeta^2 + \left[\frac{4\sqrt{2}}{3\delta_1\delta_4} + \frac{2\sqrt{2}}{\delta_2\delta_3} + \frac{2\sqrt{2}}{3\delta_3\delta_4} + \frac{2\sqrt{2}}{\delta_2\delta_4} - \frac{16B}{\delta_1\delta_4\delta_5} - \frac{8\sqrt{2}B}{\delta_3\delta_4\delta_5} + \frac{9\sqrt{2}B}{{\delta_2}^2\delta_3}\right]\nu'\zeta^2 \quad (1)$$

where ν and ν' are related to the splitting of the $^4T_2$ and a^4T_1 states due to a trigonal distortion (see Figure 12),[33] ζ is the spin−orbit coupling parameter for Cr(III), B is a Racah parameter, and the δ_i are the optical ground-state−excited-state energies as defined in Table 1. Macfarlane noted that the ground-state ZFS is ~80% due to mixing with the $^4T_2$, a^4T_1, a^2T_2, and b^2T_2 excited states in this model.[18] These

(34) Lever, A. B. P. *Inorganic Electronic Spectroscopy*; Elsevier: Amsterdam, 1984.
(35) Gamelin, D. R.; Kirk, M. L.; Stemmler, T. L.; Samudranil, P.; Armstrong, W. H.; Penner-Hahn, J. E.; Solomon, E. I. *J. Am. Chem. Soc.* **1994**, *116*, 2392.

Table 1. Optical Data for **1** in $CHCl_3$/Toluene (293 K UV/Visible and 1.8 K MCD)

UV/visible/cm^{-1} [a]	MCD/cm^{-1} [b]	assignment[c]	energy[d]	label[c]
−[e]	14 085	$^4A_2 \rightarrow {}^2E$	$9B + 3C$	
−	∼15 150	$^4A_2 \rightarrow {}^2T_1$	$9B + 3C$	
16 475	15 673	$^4A_2 \rightarrow {}^4T_2$	Δ	δ_1
	16 502	$(^4E + {}^4A_1)$		
−	20 000	$^4A_2 \rightarrow a^2T_2$	$15B + 4C$	δ_2
22 883	21 598	$^4A_2 \rightarrow a^4T_1$	$\Delta + 12B$	δ_4
	24 154	$(^4E + {}^4A_2)$		
−	27 933	$^4A_2 \rightarrow b^2T_2$	$\Delta + 9B + 3C$	δ_3
(35 000)[f]	−	$^4A_2 \rightarrow b^4T_1$	$2\Delta + 3B$	δ_5

[a] Absorption maximums from UV/visible spectrum. [b] From MCD spectrum. [c] Assignment and nomenclature from Macfarlane;[18,33] [d] Excited-state energies in terms of crystal field splitting Δ and Racah parameters. These data give $\Delta = 16475$ cm^{-1}, $B = 534$ cm^{-1}, and $C \approx 3000$ cm^{-1} and trigonal splitting parameters[33] $\nu = 1658$ cm^{-1} and $\nu' \approx 1700$ cm^{-1}. [e] Not observed. [f] Not observed, calculated from Δ and B.

expressions have been used successfully to correlate optical and EPR data for many monomeric $\{Cr(III)O_6\}$ centers including coordination complexes[36] and mineral lattices such as ruby, emerald, and spinel.[18,37]

Because the UV/visible and MCD spectra for **1** resemble those of single-ion Cr(III), we analyzed these data similarly, treating the system as a trigonally distorted (recalling the D_3 cluster symmetry), pseudomonomeric ion, to determine the *single-ion* ZFS in this cluster directly. Although there are four crystallographically independent Cr(III) sites in the crystal structure of **1**, their metrical parameters do not differ dramatically, and the differences are not resolved in the optical experiments. Therefore, at worst this approximation will give the mean single-ion optical parameters and therefore a mean single-ion ZFS for the system.

Using the assignment of the transitions given in Table 1, and the trigonal distortion parameters $\nu = 1658$ cm^{-1} and $\nu' \approx 1700$ cm^{-1} (from the experimentally observed splittings of the $^4T_2$ and a^4T_1 excited states; see Figure 12), we calculate a value of $|D| = 1.035$ cm^{-1} with $\zeta = 273$ cm^{-1} (free-ion value for Cr(III)). Calculations based on simpler models[15] that ignore mixing with spin doublet states result in much smaller values.

Solomon et al. in their work on $[FeCl_4]^-$ and $[Fe\{S(Me_4C_6H)_4\}_4]^-$ noted that analytical expressions relating the ZFS of pseudotetrahedral Fe(III) to optical excited-state energies, analogous to the treatment in eq 1 for Cr(III), can fail because of the neglect of anisotropic covalency effects.[38] Maolu and Rudowicz considered this problem explicitly for trigonally distorted Cr(III), adapting Macfarlane's model to incorporate two spin−orbit coupling parameters.[39] They found that neglect of anisotropic covalency effects leads to large errors (even in sign) in the ZFS of the $^4A_2$ ground state for Cr(III) doped in chloride and bromide lattices. However, in oxide lattices, the ZFS could be reproduced satisfactorily with a single spin−orbit coupling parameter model, because the covalency, and anisotropy in the covalency, are much less in the lighter (cf. Cl^-, Br^-) oxide host. Thus, although these effects were crucial in Solomon's study of $[FeCl_4]^-$,[38] we can neglect them in the present study (**1** can be considered as a chromium oxide core surrounded by a carboxylate shell) and use eq 1.

(ii) *g* Values. Abragam and Bleaney[15] stated that the deviation of the g values from the free electron value ($g_e = 2.0023$) in Cr(III) ions is caused by mixing of the $^4A_2$ ground state with the $^4T_2$ excited state via spin−orbit coupling:

$$g_{zz} = g_e - (8\zeta/3\Delta^4A_1)$$

$$g_{xx} = g_{yy} = g_e - (8\zeta/3\Delta^4E) \qquad (2)$$

where Δ^4A_1 and Δ^4E are the excitation energies to the trigonally split components of the $^4T_2$ excited state. When applied to simple monomeric $\{CrO_6\}$ centers such as ruby, this analysis gives g values much lower than those observed experimentally ($g = 1.98$ cf. 1.96).[12,15] However, this treatment neglects the important contribution of excited states other than $^4T_2$. Macfarlane's treatment considers the contribution from all possible excited spin quartet and spin doublet states arising from the d^3 configuration (eqs 4),[37]

$$g_{zz} = g_e - \frac{8\zeta k}{3\delta_1} + \left[\frac{-2\zeta^2(k+g_e)}{3{\delta_2}^2} + \frac{4\zeta^2(k-2g_e)}{9{\delta_3}^2} + \frac{8\zeta^2(k-2g_e)}{9{\delta_1}^2} - \frac{4\zeta^2 k}{3\delta_1\delta_2} + \frac{4\zeta^2 k}{9\delta_1\delta_3} + \frac{4\zeta^2 k}{3\delta_2\delta_3}\right] + \frac{8\zeta\nu k}{9{\delta_1}^2} - \frac{8\sqrt{2}\zeta\nu' k}{3\delta_1\delta_4}$$

$$g_{zz} - g_{xx} = \frac{4\zeta\nu k}{3{\delta_1}^2} - \frac{4\sqrt{2}\zeta\nu' k}{\delta_1\delta_4} \qquad (3)$$

where k is the orbital reduction factor that accounts for covalency. Equations 3 reproduce the magnitude and relative magnitude of the g values of Cr(III) in ruby (and other oxide lattices) much more accurately.[37] Using our optical data for **1**, we calculate the following expressions for the single-ion g values (assuming axial symmetry):

$$g_{zz} = 2.0009 - 0.0442k$$

$$g_{xx} = g_{yy} = 2.0009 - 0.0395k \qquad (4)$$

Thus, we expect $g_{zz} < g_{xx}$ for the single ions, with $g_{zz} = 1.957$ and $g_{xx} = 1.961$ in the ionic limit ($k = 1$). In Macfarlane's treatment, this is expected to lead to a negative single-ion ZFS.[37] This pattern of single-ion g values is opposite to the measured cluster g values for **1**.

Rationalization of the ZFS in the $S = 6$ Ground State of 1. The ZFS of a spin state S that results from the coupling of two individual spins S_A and S_B can be described by[8]

$$D_S = d_1D_A + d_2D_B + d_{12}D_{AB} \qquad (5)$$

where the projection coefficients d can be calculated given

(36) Andriessen, W. T. M.; Groenewege, M. P. *Inorg. Chem.* **1976**, *15*, 621.
(37) Macfarlane, R. M. *Phys. Rev. B* **1970**, *1*, 989.
(38) (a) Deaton, J. C.; Gebhard, M. S.; Koch, S. A.; Millar, M.; Solomon, E. I. *J. Am. Chem. Soc.* **1988**, *110*, 6241. (b) Deaton, J. C.; Gebhard, M. S.; Solomon, E. I. *Inorg. Chem.* **1989**, *28*, 877.
(39) Maolu, D.; Rudowicz, C. *Phys. Rev. B* **1992**, *46*, 8974.

the values of S, S_A and S_B.[8] D_A and D_B are the ZFSs of S_A and S_B, respectively, and D_{AB} is the ZFS due to the exchange (which includes the anisotropic exchange and the dipolar contributions). This vector coupling approach has been used successfully by Kremer to analyze the ZFSs of the excited spin states of antiferromagnetically coupled Cr(III) dimers where the single-ion D could be measured directly from doping Cr(III) into the isostructural and diamagnetic Co(III) dimer.[6]

Barra et al.[9] have attempted to apply this relationship to much more complicated clusters by successive coupling of spins to generate the global cluster ground-state spin. This depends on the model one chooses for the exchange coupling. For example, for Mn_{12}, the structure consists of a ring of eight Mn(III) ions surrounding a $\{Mn(IV)_4O_4\}$ cubane core.[1] The $S = 10$ ground state is often described as being the result of coupling the eight Mn(III) ions together ferromagnetically to give $S_A = 16$ and the four Mn(IV) ions together ferromagnetically to give $S_B = 6$, and then coupling these two total spins antiferromagnetically to give $S = 10$. Using eq 5 successively to generate expressions for the ZFS for $S_A = 16$, $S_B = 6$, and finally $S = 10$, they then make the assumption that the cluster ZFS will be entirely due to the single-ion ZFS of Mn(III) (which is expected to be much larger than that of Mn(IV) because of the Jahn−Teller distortion of Mn(III)); i.e., D_{AB} is assumed to be zero. Using the experimental value of the cluster ground-state ZFS (-0.46 cm^{-1}), they calculate the single-ion ZFS of the Mn(III) ions to be -2 cm^{-1}. An alternative coupling scheme gives -3.64 cm^{-1}. These values are comparable to those found in [Mn(dbm)$_3$] (-4.6 cm^{-1}) and Mn(III) doped in rutile (-3.4 cm^{-1}), both of which contain isolated $\{Mn(III)O_6\}$ centers, and thus, they conclude that the model is reasonable and that the ZFS of Mn_{12} is indeed largely due to the single-ion anisotropy of Mn(III). This analysis works because the Jahn−Teller distortion axes of all the Mn(III) ions, which are expected to define the principal axes of the *local* ZFSs, are approximately collinear with each other and with the principal axis of the *cluster* ZFS (the molecule has tetragonal symmetry). The same group has applied similar analyses to $Fe(III)_4$, $Fe(III)_6$, and $Fe(III)_8$ clusters with the conclusion that dipolar contributions to the cluster ZFS are important in these clusters.[7,11,40]

For **1** we can attempt a similar analysis but with the great advantage that we have the optically determined value for the single-ion ZFS of the Cr(III) ions. We first assume that this single-ion ZFS is valid for all Cr(III) sites. To generate a total spin of 6 in the ground state we require that, in crude terms, eight of the Cr(III) ions are "spin up" and four are "spin down". From symmetry considerations, the only logical explanation is if the spins of the central ion [Cr(1)] and the three rectangular face-capping ions (Cr(3) and symmetry equivalents, Figure 1b) are aligned with each other, but oppositely to those of the vertexes of the trigonal prism and of the triangular face-capping Cr(III) ions. We then need to define a coupling scheme to achieve this: we have tried several schemes and find that the final results do not vary a great deal and we illustrate this with two alternatives.

Table 2. Spin Projection Coefficients for Vector Coupling Scheme

S_A	S_B	S	d_1	d_2	d_{12}
$^3/_2$	$^3/_2$	3	0.200	0.200	0.300
3	$^3/_2$	$^3/_2$	2.400	0.200	−0.800
3	$^3/_2$	$^9/_2$	0.417	0.083	0.250
3	3	6	0.227	0.227	0.273
6	3	9	0.431	0.098	0.235
9	$^9/_2$	$^9/_2$	3.182	0.545	−1.364
$^9/_2$	$^3/_2$	6	0.545	0.045	0.205
$^9/_2$	$^3/_2$	3	1.833	0.083	−0.458
9	3	6	2.000	0.143	−0.571

Scheme 1. The three Cr(III) ions that lie along the cluster C_3 axis are each connected by three single-atom bridges, and we expect them to be strongly coupled. The outer two spins (Cr(2) and Cr(2A)) are aligned parallel with each other but antiparallel to the central spin (Cr(1)). The ground state of such a system is given by coupling the two outer ions to give $S = 3$ and then with the third to give $S = ^3/_2$. We then couple the three rectangular face capping Cr(III) ions (Cr(3), Cr(3A) and Cr(3B)) ferromagnetically to give $S = ^9/_2$. Equivalent vertexes of the trigonal prism (Cr(4) and Cr(4E); Cr(4A) and Cr(4D); Cr(4B) and Cr(4C)) are coupled ferromagnetically to give $S = 3$ and then coupled together ferromagnetically to give $S = 9$. The $S = 9$ and $^9/_2$ states are coupled antiferromagnetically to give $S = ^9/_2$, which is finally coupled ferromagnetically with the $S = ^3/_2$ (resulting from the three ions on the C_3 axis) to give the total ground-state spin $S = 6$.

Scheme 2. The three Cr(III) ions on the cluster C_3 axis are coupled as before. The resultant $S = ^3/_2$ is then coupled antiferromagnetically with the three rectangular face-capping ions (Cr(3), Cr(3A) and Cr(3B)), each of which is connected to Cr(1) by two single-atom bridges. This spin topology (a triangle of $S = ^3/_2$ centered on a fourth, oppositely aligned $S = ^3/_2$) is analogous to that used by Gatteschi and co-workers[11] for the $S = ^5/_2$ ions in the $Fe(III)_4$ cluster [$Fe_4(OMe)_6(dpm)_6$] (Hdpm = dipivaloylmethane) and can be treated similarly to give $S = 3$. Equivalent vertexes of the trigonal prism (which are connected by two single-atom bridges and are related by 2-fold symmetry) are coupled ferromagnetically to give a triangle of $S = 3$ states, which are then coupled together to give $S = 9$ as in scheme 1. Antiferromagnetic coupling of this $S = 9$ with the $S = 3$ gives the final spin of $S = 6$.

The d projection coefficients required for all these calculations, obtained by the method detailed by Bencini and Gatteschi,[8] are in Table 2. However, **D** is a tensor quantity related to its diagonal elements by

$$D = D_{zz} + (D_{xx} + D_{yy})/2$$

and

$$D_{xx} + D_{yy} + D_{zz} = 0 \qquad (6)$$

Therefore, we must consider the relative orientations of the

(40) (a) Barra, A.-L.; Gatteschi, D.; Sessoli, R. *Chem. Eur. J.* **2000**, *6*, 1608. (b) Gatteschi, D.; Sorace, L. *J. Solid State Chem.* **2001**, *159*, 253.

local and cluster magnetic axes before we can use these coefficients to calculate the single-ion contribution to the cluster ground-state ZFS. In the following discussion, D_{ii} are diagonal elements of the *local* **D** tensors (hence, *x*, *y*, *z* does not imply a common coordinate frame), and D_{II} are diagonal elements of the *cluster* $\mathbf{D}_{S=6}$ tensor (*X*, *Y*, *Z* coordinate frame). Equations 6 give the component of a **D** tensor along its *z* axis as $D_{zz} = 2D/3$, and in the assumption of axial symmetry, the in-plane component, $D_{xx} = D_{yy} = -D_{zz}/2$, is half the magnitude and opposite in sign to D_{zz}.

1 has crystallographic D_3 symmetry and the unique axis of the $S = 6$ ground-state ZFS (D_{ZZ}) is required to be parallel to the C_3 axis. The trigonal face capping and the central Cr(III) ions lie on the C_3 axis and therefore their local D_{zz} axes must be collinear with each other and with the C_3 axis; i.e., their D_{zz} values project directly onto D_{ZZ} (Figure 1b). Each of the rectangular face-capping Cr(III) ions lie on a C_2 axis and their D_{zz} axes will be collinear with these in the approximation of axial local symmetry. These C_2 axes are perpendicular to the cluster C_3 axis and hence only the in-plane D_{xx} components of their ZFSs project onto the cluster D_{ZZ}. The vertexes of the trigonal prism do not lie on any symmetry element but are all related by symmetry. Analysis of the coordinates of the local $\{CrO_6\}$ coordination geometry[22] shows that there is a statistically significant elongation of one of the axes, along the Cr(4)−O(2) and Cr(4)−O(1A) bonds, which we assign as the local *z* axis. There is no marked trigonal compression along any of the octahedral faces. Therefore, we assume that the local D_{zz} axes for these sites are parallel to the O(2)−O(1A) vectors. These are nearly perpendicular to the cluster C_3 axis (93°), so effectively, only the in-plane D_{xx} components project onto the cluster D_{ZZ}.

Thus when the single-ion ZFSs from the Cr(III) ions lying on the C_3 axis are used in eq 5, the coefficients in Table 2 must be used with D_{zz}, while the D_{xx} value is appropriate for all the other sites. If we assume that the cluster ZFS is entirely single ion in origin, i.e., we assume $D_{AB} = 0$ at each stage of the calculation, then using scheme 1 we have

$$D_{ZZ} = 0.279D_{xx} + 0.052D_{zz} \tag{7a}$$

And for scheme 2

$$D_{ZZ} = 0.301D_{xx} + 0.014D_{zz} \tag{7b}$$

Using the optically determined value for the local ZFS of $D = \pm 1.035$ cm^{-1}, we have $D_{zz} = \pm 0.693$ cm^{-1} and $D_{xx} = \pm 0.347$ cm^{-1}. Scheme 1 gives $D_{ZZ} = \pm 0.061$ cm^{-1}, which corresponds to a ZFS of $D_{S=6} = \pm 0.091$ cm^{-1} for the $S = 6$ ground state of the cluster. This is in remarkable agreement with the experimentally determined value of $+0.088$ cm^{-1}. Scheme 2 gives $D_{S=6} = \pm 0.142$ cm^{-1}. The positive sign of the experimental cluster $D_{S=6}$ (determined by HF-EPR) implies that the single-ion ZFS is negative: this is consistent with the experimentally determined sign for isolated, trigonally distorted $\{CrO_6\}$ centers such as in ruby[15] and with the calculated pattern of the single-ion *g* values ($g_{zz} < g_{xx}$, see above).

The vector coupling approach can also be applied to the calculated single-ion *g* values via[8]

$$g_S = c_1 g_A + c_2 g_B \tag{8}$$

where g_A and g_B are the *g* values of centers A and B, and the projection coefficients c can be calculated from *S*, S_A, and S_B. Using either coupling scheme 1 or 2 above, and taking into account the relative orientations of the local and global axes as before, gives the following expressions for the cluster $S = 6$ ground-state *g* values:

$$g_{ZZ} = (3/4)g_{xx} + (1/4)g_{zz}$$

$$g_{XX} = (1/4)g_{xx} + (3/4)g_{zz} \tag{9}$$

Hence, substituting eqs 4 into 9 we have

$$g_{ZZ} = 2.0009 - 0.0407k$$

$$g_{XX} = 2.0009 - 0.0430k \tag{10}$$

Note that, in contrast to the single-ion *g* values, the expected pattern for the cluster *g* values is $g_{ZZ} > g_{XX}$. This is in agreement with the experimental EPR data. Thus, the above analysis using Macfarlane's treatment to calculate the single-ion spin Hamiltonian parameters, and the vector coupling approach to reproduce the cluster parameters, is self-consistent. The calculated cluster *g* values in the ionic limit ($k = 1$) are $g_{ZZ} = 1.960$ and $g_{XX} = 1.958$, which are in good agreement, albeit slightly low, compared to the experimental $g_{ZZ} = 1.965$ and $g_{XX} = 1.960$. If we use these experimental values to estimate the covalency parameter via eqs 10, we get $k \approx 0.9$. This is very high compared to that Macfarlane assumed for, e.g., ruby ($\sim$0.7),[37] but is consistent with the low covalency of Cr(III) ions in oxide lattices discussed by Rudowicz.[39] If we then include this covalency in the calculation of the single-ion ZFS (and hence the cluster ground-state ZFS) in the form of a reduced spin−orbit coupling parameter (recalling that *D* is proportional to ζ^2),[18,37] we get values of $D_{S=6}$ in the range 0.074−0.115 cm^{-1}. If we assume the same covalency as Macfarlane assumed for ruby,[37] we get the range 0.045−0.069 cm^{-1}. The simultaneous reproduction of the experimental *g* and *D* values of **1** from optical data gives confidence in the validity of the method.

The range of calculated $D_{S=6}$-values are in very good agreement with experiment ($+0.088$ cm^{-1}), and we conclude that the ZFS in the ground state of **1** is almost entirely due to the single-ion ZFS of the constituent Cr(III) ions. These results are consistent with Kremer's studies on Cr(III) dimers where the single-ion ZFS was found to be $\sim$1 order of magnitude larger than the anisotropic exchange contributions to the cluster ZFSs.[6] If we had simply assumed the single-ion ZFS in **1** to be similar to that in ruby or in a monomeric $\{CrO_6\}$ complex such as [Cr(acac)$_3$] (Hacac = acetylacetonate), we would calculate cluster ZFSs that are under half that of the true value, and this demonstrates the value of determining the single-ion ZFSs directly.

The fact that the cluster ZFS has *opposite sign* to that of its component single ions is a result of the relative orientations of the local and cluster magnetic axes: all but 3 of the 12 Cr(III) ions project the in-plane, positive component of their ***D*** tensors onto the unique cluster axis. Other workers have also noted the importance of the orientation of magnetic axes. Christou, Hendrickson, and co-workers have demonstrated that the effective barriers to relaxation of magnetization can be very different between isomeric Mn_{12} derivatives that differ only in the orientation of *one* of the local Mn(III) Jahn−Teller axes ("Jahn−Teller isomerism").[41] However, no quantitative relationship between $D_{S=10}$ and the relative orientation was found.[42] Caneschi et al. have analyzed the ZFS of the $S = 1$ excited state of $[Fe_6(OCH_3)_{12}(pmdbm)_6]$ on the basis that the principal axes of the local ZFSs are perpendicular to that of the cluster.[43] However, the predominantly antiferromagnetic coupling in that case results in negative projection coefficients, and thus, the ($S = 1$ excited state) cluster and local ZFSs still have the *same* sign. The work presented here gives a clear example of a cluster having a large spin ground-state ZFS of a sign opposite to that of its single ions. This demonstrates that in the design of molecules with the large negative ZFSs necessary for SMM behavior, the alignment of the single-ion magnetic axes relative to each other and to the cluster axes is *as important* as the sign of the single-ion ZFS. Mn_{12} has a large negative ZFS because the local Mn(III) distortion axes, where the single-ion ZFS is negative, are approximately parallel to each other and the cluster C_4 axis.[1,9,41] A SMM could be made from a metal ion with a positive ZFS if it could be engineered such that the local principal axes were perpendicular to that of the cluster. If the single-ion ZFS in this study was positive, then **1** would be a SMM.

(41) (a) Sun, Z.; Ruiz, D.; Dilley, N. R.; Soler, M.; Ribas, J.; Folting, K.; Maple, M. B.; Christou, G.; Hendrickson, D. N. *Chem. Commun.* **1999**, 1973. (b) Aubin, S. M. J.; Sun, Z.; Eppley, H. J.; Rumberger, E. M.; Guzei, I. A.; Folting, K.; Gantzel, P. K.; Rheingold, A. L.; Christou, G.; Hendrickson, D. N. *Inorg. Chem.* **2001**, *40*, 2127.

(42) Aubin, S. M. J.; Sun, Z.; Rumberger, E. M.; Hendrickson, D. N.; Christou, G. *J. Appl. Phys.* **2002**, *91*, 7158.

(43) Caneschi, A.; Cornia, A.; Fabretti, A. C.; Foner, S.; Gatteschi, D.; Grandi, R.; Schenetti, L. *Chem. Eur. J.* **1996**, *2*, 1379.

Conclusions

We have demonstrated by multifrequency EPR spectroscopy that **1** has an $S = 6$ ground state and that the ZFS within this ground state is $+0.088$ cm^{-1}. This is supported by micro-SQUID magnetization measurements on single crystals of **1** that show a stepped structure because of M_S energy level crossings solely within the ground state. Unfortunately, the positive sign of the ZFS negates the possibility of **1** behaving as a SMM.

We have shown that the single-ion ZFS in a geometrically complicated cluster, where synthesis of diamagnetic analogues for doping experiments is impossible, can be directly determined from high-quality optical data (e.g., low-temperature MCD). Using this information and a vector coupling approach, we have shown that the ground-state ZFS of **1** is almost entirely single ion in origin and have calculated g values consistent with experiment. More importantly, we have shown that the relative orientations of the local and cluster magnetic axes can lead to a cluster ZFS opposite in sign to the single ion, even when this is the only significant contribution. This implies that SMM research need not be restricted to the use of metal ions that give rise to negative ZFSs.

Acknowledgment. We thank the EPSRC (UK) for funding of the EPR Service at Manchester and St. Andrews and for studentship (S.P.) and postdoctoral (M.M.) grants. The collaboration between Manchester and Kishinev has been supported by INTAS (Contract 00-0172), and The Royal Society provided support for an Ex-Agreement Fellowship (G.A.T.). We are also grateful to the EU-TMR "MolNanoMag" for support, and for an OSS award to G.R.

IC034541B